POLITECNICO DI TORINO

Master's Degree in Communications and Computer Networks Engineering

Master's Degree Thesis

Different ways of enforcing Love's condition in determining equivalent currents from radiated field data

Supervisors

Prof. Giuseppe VECCHI

Dr. Marco RIGHERO

Dr. Giorgio GIORDANENGO

Candidate

Tianle HAO

April 2022

Abstract

The main objective of this thesis is the study of three possible ways of determining equivalent currents from radiated field samples solving an inverse problem. The results obtained using the three different formulations are compared with reference results. As we work with synthetic data, we can access true values of the radiated field at an arbitrary location. From that, we can also evaluate true equivalent currents fulfilling Love's condition. These constitute reference values. As currents fulfilling Love's null field condition are directly related to the tangential components of the field at those locations, they are useful for diagnostic purposes. We consider three sets of equivalent electric and magnetic currents, each one obtained solving an inverse problem satisfying different equations. The first method enforces that the sought currents radiate a field match the field samples at the measurement surface. The second method enforces concurrently both the previous condition and the condition of having a vanishing field inside the reconstruction surface. The third method derives currents fulfilling Love's condition applying a projection operator to the currents obtained with the first method. The results obtained during the work of the thesis show that the inverse currents obtained with the third method have the smallest error with respect to the reference currents. However, these currents radiate a field that differs from the reference one for an amount larger than in the cases of the other two methods. The currents obtained with the second method are the best trade-off between accuracy of the re-irradiated field and the adherence with the true equivalent currents fulfilling Love's condition. These results hold for different values of Signal to Noise Ratio.

Acknowledgements

Throughout the writing of this dissertation I have received a great deal of support and assistance.

I would first like to thank my supervisor, prof. Giuseppe Vecchi, whose expertise was invaluable in formulating the research questions and methodology. Your insightful feedback pushed me to sharpen my thinking and brought my work to a higher level.

I would also like to thank my tutors, Marco Righero and Giorgio Giordanengo, for their valuable guidance throughout my studies. You provided me with the tools that I needed to choose the right direction and successfully complete my dissertation.

In addition, I would like to thank my parents for their wise counsel and sympathetic ear. You are always there for me.

Finally, I could not have completed this dissertation without the support of my friends, LiuXin, who provided stimulating discussions as well as happy distractions to rest my mind outside of my research.

Table of Contents

List of Tables

List of Figures

Chapter 1

INTRODUCTION

As technology develops, the issue of source reconstruction, which is closely related to a range of practical applications such as antenna diagnostics from field measurements, compact antenna representation and near-field to far-field (NF-FF) conversion, is also maturing. The aim of source reconstruction is to determine a set of equivalent currents from measured field samples at known locations. We describe here some previous works on this topic in chronological order. In [1], the authors present the method applied to the evaluation of the radiation from commercial antennas at any observation point. The work in [2] describes an Integral Equation algorithm that allows the characterization of antennas of complex geometry both for near field to far field (NF-FF) transformation purposes as well as for diagnostic tasks. [3] uses a field based algorithm that enables the determination of the actual complex excitation levels from spherical near-field data that is used to calculate the desired far field employing a near-field to far-field transformation. In [4], the authors use a formulation for the Inverse Scattering Problem to improve the resolution for the equivalent sources characterization. [5] discusses how to avoid Undesired interactions affect of the source reconstruction technique. [6] presents a novel formulation of the source reconstruction problem on arbitrary three-dimensional (3-D) surfaces based on integral equations. In [7] the authors introduce the meaning of Love's equivalence (also called zero-interior field) and different formulations of the inverse-source problem whereby from the knowledge of complex vector electric field data at a specified exterior surface to acquire equivalent sources and fields. Finally, for improving the performance when control the the solution process, formulations and iterative solutions are presented [8].

The major goal of this work is to compare three possible ways of determining equivalent currents from radiated field samples and clarify their performance at different levels of Signal to Noise Ratio(SNR). Reviewing the available literature, various formulations of the inverse equivalent surface-source problem and corresponding solution approaches are discussed and investigated. Based on these essays,

by importing the designed antenna model with known parameters in Matlab and comparing the results, this work summarises their performance in a set SNR range and their degree of accuracy at the same SNR.

The paper is organized as follows. Chapter 2 focuses on true Love current as a reference quantity and the logic and formulation for the three different equivalent inverse currents. Chapter 3 determines the performance of the three operators by means of the mean and variance of the current, power and field on the reconstructed surface. Chapter 4 compares the radiation field variation of four equivalent inverse currents on a specified surface by means of an increase SNR. Chapter 5 provides a description of the three methods in terms of their performance of running time.

This portion of work in my thesis will contribute to the development of work related to the Fast testing of Antennas with hybrid Measurement and Simulations.

Chapter 2

Inverse equivalent surface-source solution

Consider an inverse equivalent surface-source formulation as depicted in Fig 2.1. The input data for the problem are the values of the electric field tangent to a specified measurement surface denoted by Σ_M, Σ_M is a sphere or cylinder closed surface which is in general located in some distance far from reconstruct surface Σ_R. The surface sources on the surface Σ_R are equivalent sources representing the radiation fields of all sources within the enclosed Antenna Under Test (AUT). Normally quantities of AUT is unknown, however, here we are working in a simulated controlled environment, to check the accuracy of the algorithms, so we insert an AUT whose parameters we know and whose radiated field we are able to evaluate at arbitrary locations, (reference field). J_{eq} and M_{eq} are the equivalent electric and magnetic current on the closed surface Σ_R. E_+ and H_+ are external fields remain unchanged, but for the inner fields E_- and H_- substituted by E_-' and H_-'. For satisfied the equivalent problem, the fields and currents above must obey the equation below:

$$\begin{cases} \hat{n} \times [H_+(r) - H'_-(r)] = J_{eq} \\ -\hat{n} \times [E_+(r) - E'_-(r)] = M_{eq} \end{cases} \quad r \in \Sigma_R \tag{2.1}$$

Where $\hat{n}$ is the unit normal vector on surface Σ_R. Consider that .J_{eq} and M_{eq} are radiated in an unbounded homogeneous space and for equivalent problem the material of the region within surface R is removed, So irrespective of the part of the internal fields E_- and H_-, the fields radiated on measurement surface Σ_M by the equivalent current on reconstruction surface Σ_R is only depending on the external fields E_+ and H_+. The fields can be computed by using the conventional free-space radiation operator which follows:

$$\hat{n} \times E(r) = \hat{n} \times [-\eta_0 \mathcal{L}(J_{eq}; r) + \mathcal{K}(M_{eq}; r)] r \in \Sigma_M \tag{2.2}$$

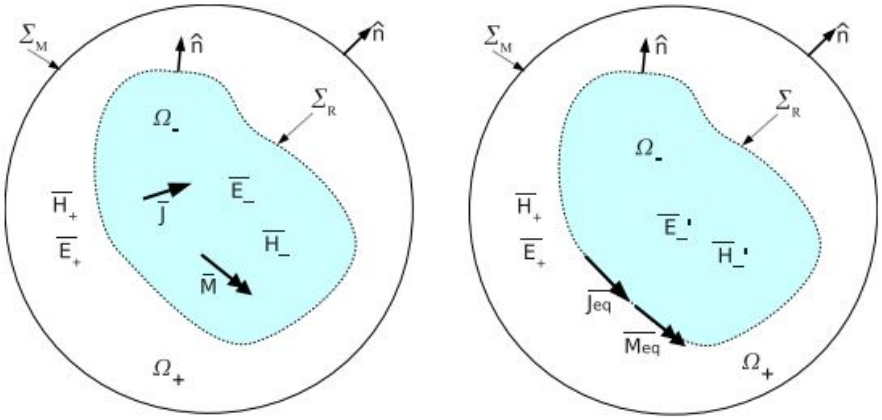

Figure 2.1: Equivalent principle. Figure taken from [7]

where

$$\mathcal{L}(J_{eq};r) = jk_0 \int_{\Sigma R} [J_{eq}(r') + \frac{1}{k_0^2} \bigtriangledown \bigtriangledown_s'] \times g(r,r')ds' \tag{2.3}$$

$$\mathcal{K}(M_{eq};r) = \int_{\Sigma R} M_{eq}(r') \times \bigtriangledown_{g(r,r')ds'} \tag{2.4}$$

$$g(r,r') = \frac{e^{-jk_0|r-r'|}}{4\pi|r-r'|} \tag{2.5}$$

$$\eta_0 = \sqrt{\mu_0/\epsilon_0}, k_0 = \omega\sqrt{\mu_0\epsilon_0} \tag{2.6}$$

and $\bigtriangledown_s^{'}$ is the surface divergence operator($r \notin \Sigma R$).

2.1 Introduction of Love's current

The function of forward operator can map the electric and magnetic current distribution of closed reconstruction surface Σ_R to the fields samples on measurement surface Σ_M. The purpose of using the forward operator is obtain the equivalent currents which can radiate a field same like the field samples on Σ_M , or at least make the norm difference between the output fields with the real fields on measurement surface minimized. In this simulation, the samples collected on the measurement surface Σ_M are known, so according to the forward operator, the equivalent electromagnetic current on the reconstruction surface Σ_R can be computed. The results should be compared with the reference ones obtained from Love currents computed directly from the simulation of the antenna. Before we

introduce the three operators, it is necessary to know about zero-field or *Love* condition as the reference in this experiment which satisfied the equations as follows:

$$\begin{cases} \hat{n} \times H_+(r) = J_{eq}^{Love} \\ -\hat{n} \times E_+(r) = M_{eq}^{Love} \end{cases} \quad r \in \Sigma_R \tag{2.7}$$

On reconstruction surface Σ_R, the equivalent electric and magnetic current radiated by AUT which inserted in interior region will set the interior field equal to zero. With Love 's equivalence equations, fields in the boundary are obtained directly from the equivalent currents.

2.2 Introduction of 3 kinds of operator

1. In the simplest case, The operator mapping the equivalent electric and magnetic current densities J_{eq}^F and M_{eq}^F on reconstruction surface Σ_R to field samples on measurement surface at a certain distance. This case is called *fitting* which satisfied the equations below:

$$\left\{ E(J_{eq}^F) + E(M_{eq}^F) = E(r) \quad r \in \Sigma_M \right. \tag{2.8}$$

2. The second kind of operator considers additional constraints to the inverse source problem and is made of two parts: one part of it is the operator mapping a surface current to field samples on a measurement surface at a certain distance from the reconstruction surface, same like *fitting* case. Another part is the operator mapping the equivalent current on reconstruction surface Σ_R to field samples which collected on the same surface Σ_R which should be 0. This case is called *loveside*. The equivalent electromagnetic surface current densities are defined as J_{eq}^S and M_{eq}^S.

$$\begin{cases} E(J_{eq}^S) + E(M_{eq}^S) = E(r) \\ E(J_{eq}^S) + E(M_{eq}^S) = E(r') = 0 \end{cases} \quad r \in \Sigma_M, r' \in \Sigma_R \tag{2.9}$$

3. In the considered case of electromagnetic inverse source, the third possibility also be examined: firstly force the equivalent electromagnetic current densities on reconstruction surface Σ_R matching of the field samples (same as in *fitting* case), then evaluate the field radiated on the reconstruction surface by these electromagnetic inverse currents and at the last step evaluate the *Love* currents from these fields. This case is called *lovepost*. The equivalent electromagnetic current densities defined as J_{eq}^P and M_{eq}^P in this case and they satisfy the

equation below.

$$\begin{cases} E(J^F_{eq}) + E(M^F_{eq}) = E(r) \\ J^P_{eq} = n \times (H(J^F_{eq}) + H(J^F_{eq})) \\ M^P_{eq} = -n \times (E(J^F_{eq}) + E(J^F_{eq})) \end{cases} \qquad r \in \Sigma_M, r' \in \Sigma_R \tag{2.10}$$

where n is the outward normal to Σ_R.

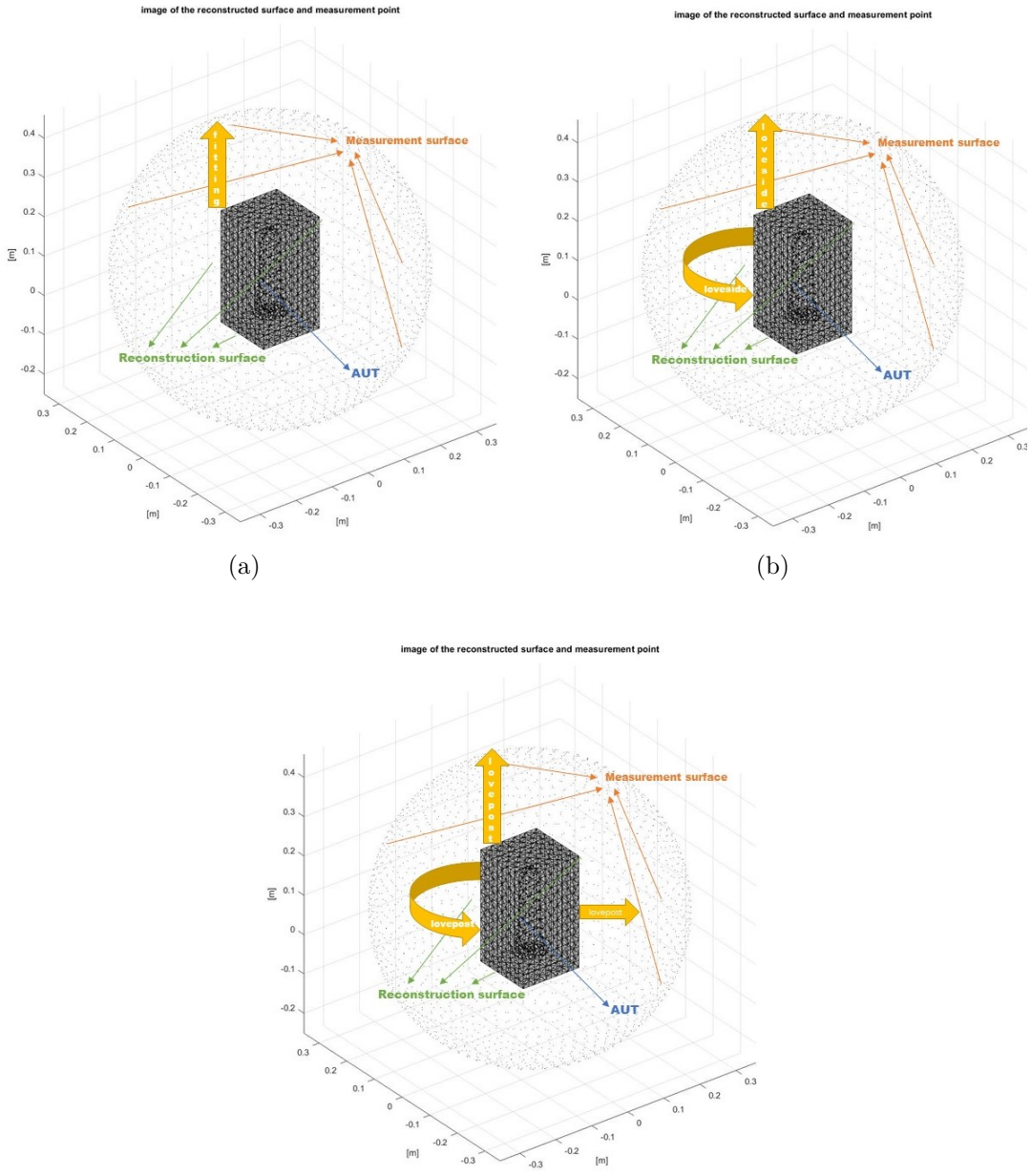

Figure 2.2: The logical principle of 3 operators: (a) Fitting, (b) Loveside, (c) Lovepost.

Chapter 3

ON FAR FIELD

In this section, we investigate anti-interference performance of *Fitting*, *Loveside* and *Lovespost* by adding noise interference to the simulated environment and comparing the equivalent currents obtained from these three operators at the reconstruction surface (Far field surface) with those obtained from love current. The range of SNR value is [30 35 40 45 50 55 60]. Since multiple experiments as noise is something random, in order to obtain the result with greater precision and higher accuracy, for each value of SNR the experiments repeat 20 times. For each case (*Fitting*, *Loveside* and *Lovespost*) inverse source currents, field radiated by the inverse source currents and the power flux and power density of these fields should be computed.

1. Inverse source currents

   It can be seen from Fig 3.1(a) and Fig 3.1(b) that the difference in mean value and variance of real part and imaginary part of current of *Fitting*, *Loveside* and *Lovespost* showed a stable trend within the SNR range 30-60. Overall, *Lovespost* is the best performer, with the smallest error between the current magnitude and the reference current obtained through it, followed by *Loveside*, which also has a small error, and finally *Fitting*, which has the largest error, almost four times that of *Lovespost*. For *Fitting* and *Loveside*, their imaginary parts show a smaller difference than in the case of real part of the same SNR value simulation. For *Lovespost*, it is good enough that there is no great difference between its real part and its imaginary part.

2. The Power flux and power density of these fields

   It can be seen from Fig 3.2(a) and Fig 3.2(b) that in general the mean value and variance of three operators' real power flux shown a stable trend as the SNR increases. Among them, *Fitting* has the biggest difference with *truelove* then followed by *Lovepost*. The difference between "*Loveside* and truelove is

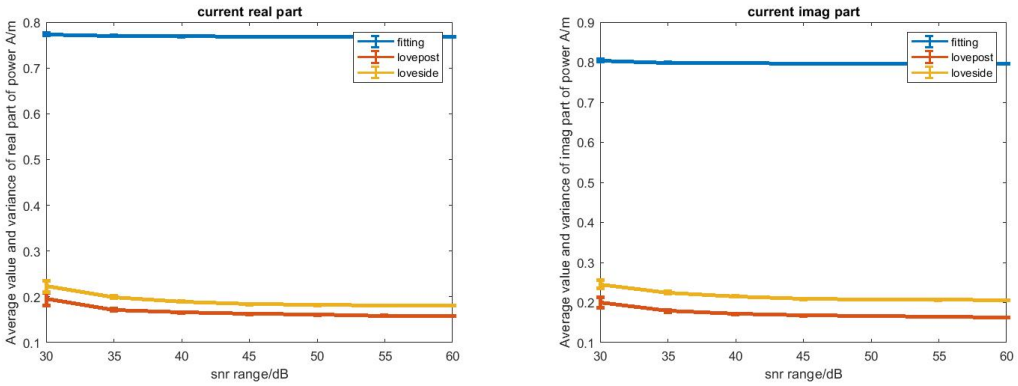

(a) (b)

Figure 3.1: *Fitting* refers to the J_{eq}^{F} in Eq(2.8), *Loveside* refers to the J_{eq}^{S} in Eq(2.9), *Lovepost* refers to the J_{eq}^{P} in Eq(2.10). The difference between the reference current from 3 kinds of equivalent inverse current.(a)Real part of current(b)Imaginary part of current

minimal. It can be seen from Figure 3.2(a) that the real part of the power flux for the three operators is a horizontal straight line, indicating that this parameter is not affected by the SNR familiarity. As can be seen from Fig 3.2(b), the error in power flux increases for all three operators as the value of SNR increases to 45, and then decreases as SNR continues to increase to 60.

3. Field radiated by the inverse source currents on reconstructed surface

   As showed in Fig 3.3, with the increase of SNR, the difference of mean and variance of fields obtained by *Fitting*, *Loveside* and *Lovepost* on reconstruction surface shows a decreasing trend. Among them, as the SNR increases to 40, *Lovepost* shows a slow decline, and when the SNR is greater than 40, it maintains an error of 12mV/m. In contrast, the errors in *Fitting* and *Loveside* show the same linear proportional decrease with SNR, their curves almost coincide, and when the value of SNR reaches 60, the reconstructed fields obtained by these two operators have almost no error with the reference field.

4. The fields radiated by equivalent currents on measurement surface Σ_R

   CO and CX refer to co-polarized and cross-polarized components of the field radiated by the antenna. In this case CO is the left-handed circular polarization and CX is the right-handed circular polarization. All the figures got at SNR equal to 60. As shown in Fig 3.4, when the SNR is set to 60 in the simulation,

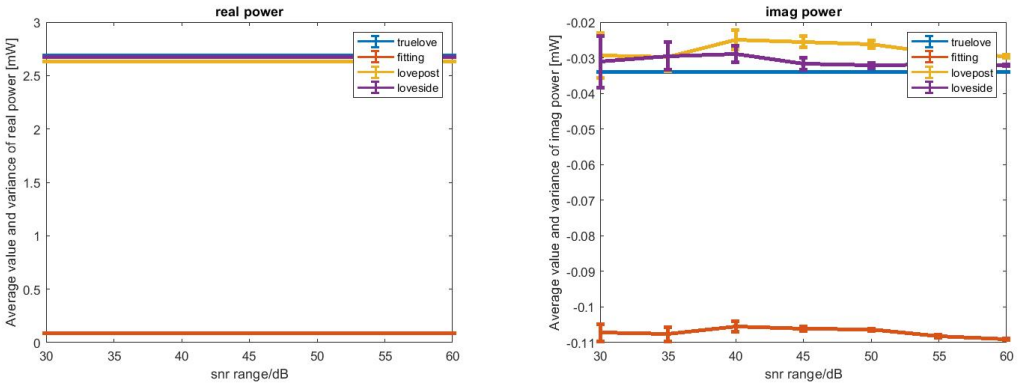

(a) (b)

Figure 3.2: *Fitting* refers to the J_{eq}^{F} in Eq(2.8),*Loveside* refers to the J_{eq}^{S} in Eq(2.9), *Lovepost* refers to the J_{eq}^{P} in Eq(2.10). The difference from the reference power flux from the power flux of 3 kinds of operators (a) Real part (b) Imaginary part.

there is no visible difference between the reconstructed field and the reference field obtained at the far field by the three equivalent inverse currents.

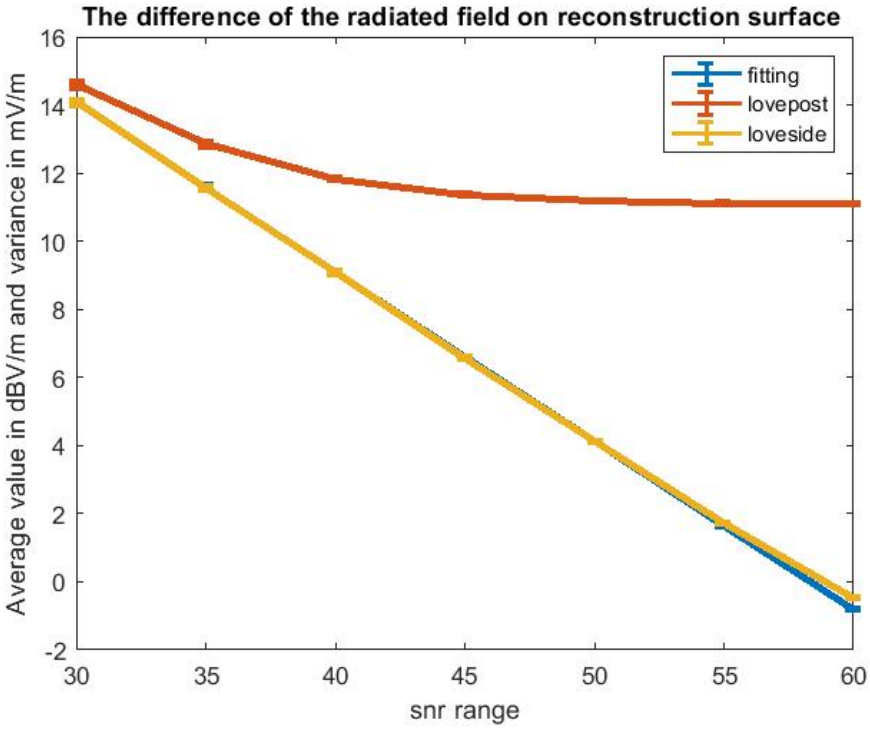

Figure 3.3: *Fitting* refers to the J_{eq}^{F} in Eq(2.8), *Loveside* refers to the J_{eq}^{S} in Eq(2.9), *Lovepost* refers to the J_{eq}^{P} in Eq(2.10). The difference form the reference field and the field reconstructed by 3 forwarders on reconstruction surface

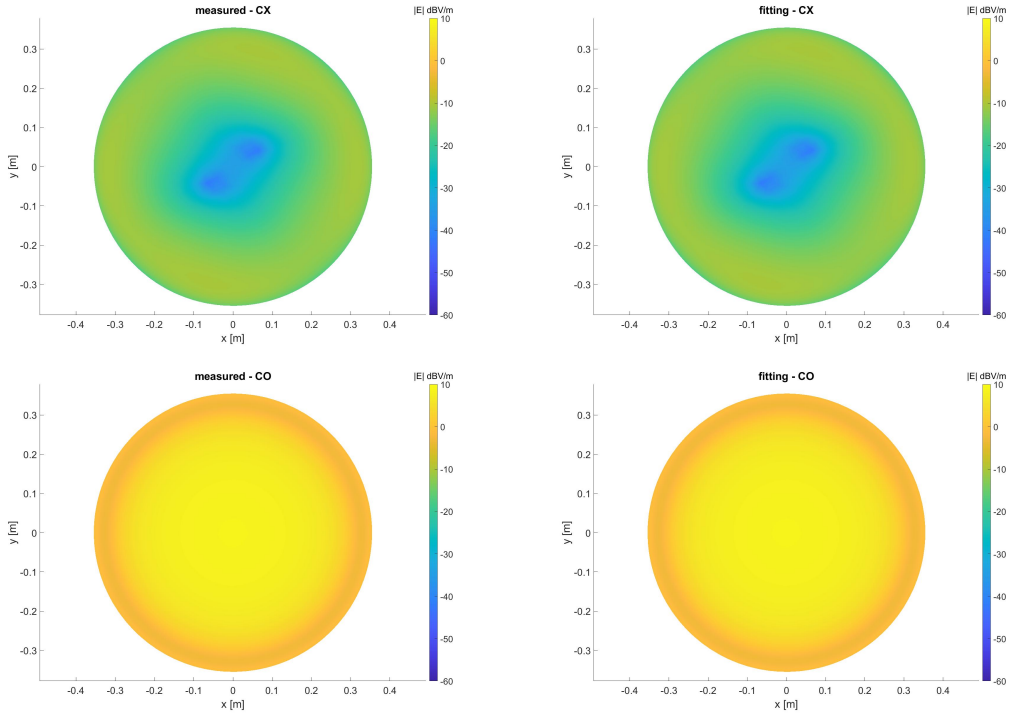

(a) (b)

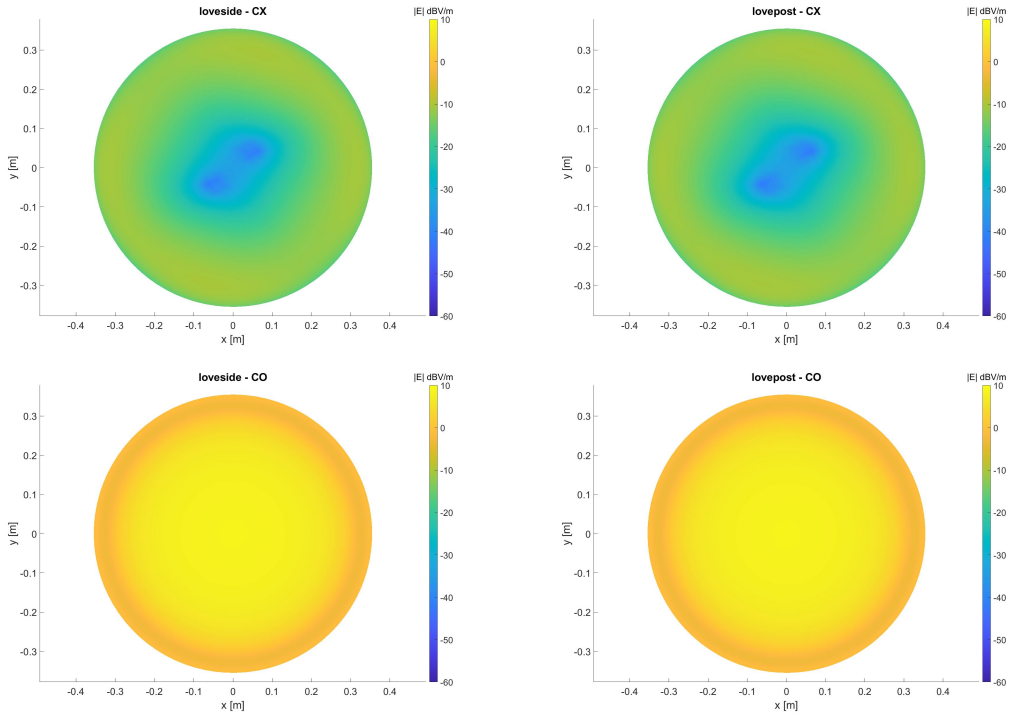

(c) (d)

Figure 3.4: Field radiated on the measurement surface when SNR set to 60. *Measured* refers to the J_{eq}^{Love} in Eq(2.7), *Fitting* refers to the J_{eq}^{F} in Eq(2.8), *Loveside* refers to the J_{eq}^{S} in Eq(2.9), *Lovepost* refers to the J_{eq}^{P} in Eq(2.10). (a)True love(b)Fitting(c)Loveside(d)Lovepost.

Chapter 4

ON NEAR FIELD

Another enclosed surface Σ_T (Near field surface) which is near reconstruction surface Σ_R is built as depicted in Fig 4.1. In this chapter we focus on exploring the performance of 3 different forward operators (Fitting, Loveside, Lovepost) against the noise when radiate the barycentre points on test surface Σ_T. Cause the quantities of AUT are known, the location of the points to be radiated is known, the electric field and magnetic field can be computed as reference fields, which be used to compare with the fields radiated by *Fitting*, *Loveside* and *Lovepost* inverse equivalent currents.

1. Norm difference in fields

   Comparing the pictures Fig 4.2 (a) and Fig 4.2 (b) we can see that the norm difference ratio of 3 operators in magnetic field and electric field have the same trend, both decrease with the increase of SNR, within the SNR range 30-35, all their norm difference decreases fast, in the range of SNR from 35-45 the curves of *Fitting* and *Loveside* still decrease fast, but for *Lovepost* the decrease is more flat, and when the SNR increases to larger than 45, the norm The decreasing trend of *Fitting* and *Loveside* difference ratio slows down. In the interval of SNR from 30 to 60, Looking at the curves in the figure, we can see that the norm difference between the radiation field on the test surface by *Fitting* and the reference current on the test surface is the smallest, followed by *Loveside*, and the largest error is *Lovepost*.

   When the SNR is set to 30, the norm difference ratio for *Fitting* is roughly 2.1%, and it drops from 0.8% to about 0.6% when the value of SNR increase from 45 to 60. For the *Loveside*, it shows the greatest change in the interval from 30 to 45 SNR, dropping from 2.4% to 1%, after which it tends to flatten out, reaching 60 SNR at 0.9%. The norm difference ratio for *Lovepost* is around 2.6% when SNR equal to 30, then decrease to 1.8% when SNR is 60.

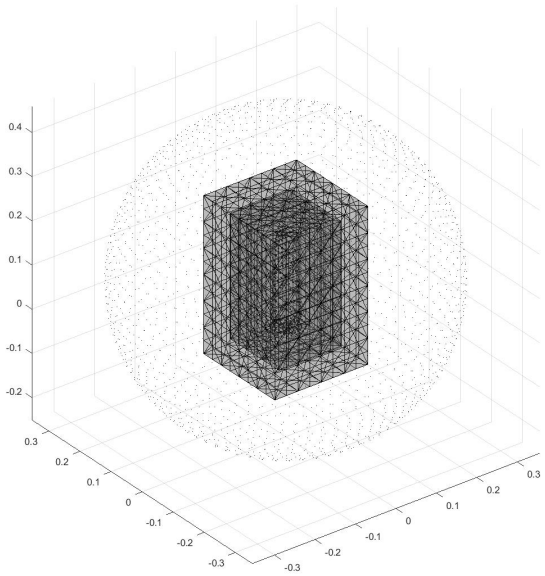

Figure 4.1: Reconstruction surface Σ_R, Test surface Σ_T and Measurement surface Σ_M. The reconstructed field Σ_R verifies the performance performance of the three methods in the far field, while the test surface Σ_T is used to verify their performance in the near field, and the measurement surface Σ_M is the surface which the radiation samples are collected in the experiment.

2. Fields on far field

   As shown is Fig 4.3-4.6, when the SNR is set to 30 and the radiation field of *Fitting*, *Loveside* and *Lovepost* on the test surface is compared with the reference field, it is already very good.

3. difference in fields

   As shown in Fig 4.7, when set SNR equal to 30, the radiation field at the test surface is discussed in two cases. In the electric field, the overall error in *Fitting* is in the [-25 -20] dB range, the overall error in *Loveside* and *Lovepost* is in the [-25 -20] dB range, but some of these are in the [-15 -10] dB range. In the magnetic field, the overall error for *Fitting* is in the [-80 -70] dB range and the overall error for *Loveside* and *Lovepost* is in the [-70 -65] dB range.

   From Fig 4.8 we can see that when SNR equal to 45, in the electric field, the overall error of *Fitting* and *Loveside* is in the range of [-35 -20] dB, and the overall error of *Lovepost* is in the range of [-25 -15] dB. In the magnetic field,

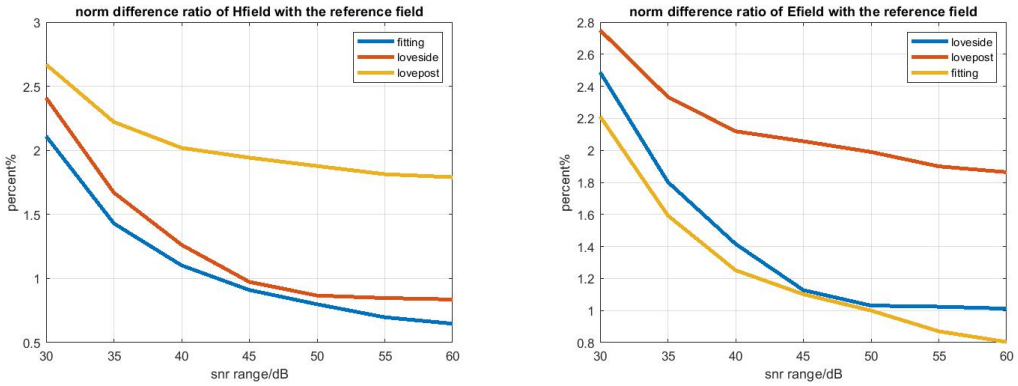

(a) (b)

Figure 4.2: The norm difference of field radiated by J_{eq}^{F} and M_{eq}^{F}, J_{eq}^{S} and M_{eq}^{S}, J_{eq}^{P} and M_{eq}^{P} with the reference field on measurement surface. (a)Magnetic field(b)Electric field

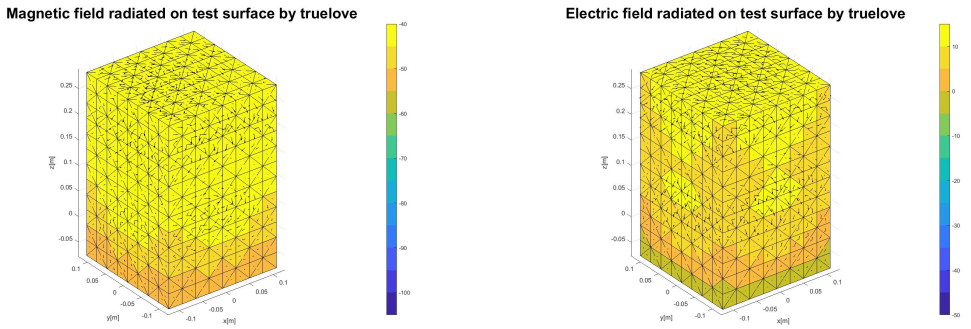

(a) (b)

Figure 4.3: The fields radiated by reference current(true love current) on test surface. *TrueLove* refers to the J_{eq}^{Love} in Eq(2.7), (a)Magnetic field(b)Electric field

the overall error of *Fitting* and *Loveside* is in the range of [-95 -75] dB, and the overall error of *Lovepost* is [-80 -65] dB. Fig 4.9 shows SNR equal to 60, the radiation field at the test surface is discussed in two cases. In the electric field, the overall error for *Fitting* and *Loveside* is in the range of [-40 -25] dB and the overall error for *Lovepost* is in the range of [-30 -20] dB. In the magnetic field, the overall error of *Fitting* and *Loveside* is in the range of [-95 -80] dB, and the overall error of *Lovepost* is [-85 -70] dB. As the SNR increases, the error in the radiation field on the T surface decreases, with *Lovepost* showing the worst performance with the biggest error among them.

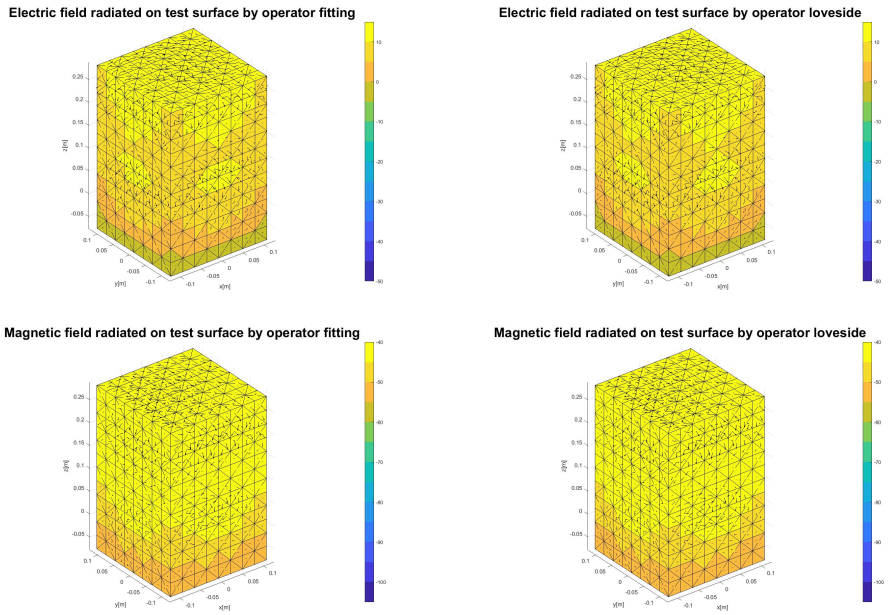

(a) (b)

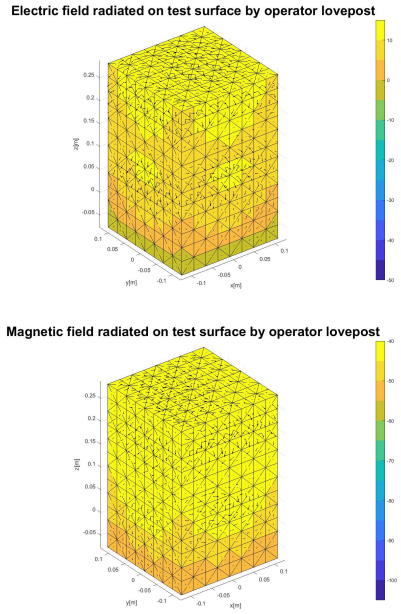

(c)

Figure 4.4: Field radiated on test surface when SNR set to 30.*Fitting* refers to the J_{eq}^{F} in Eq(2.8),*Loveside* refers to the J_{eq}^{S} in Eq(2.9),*Lovepost* refers to the J_{eq}^{P} in Eq(2.10). (a)Fitting(b)Loveside(c)Lovepost.

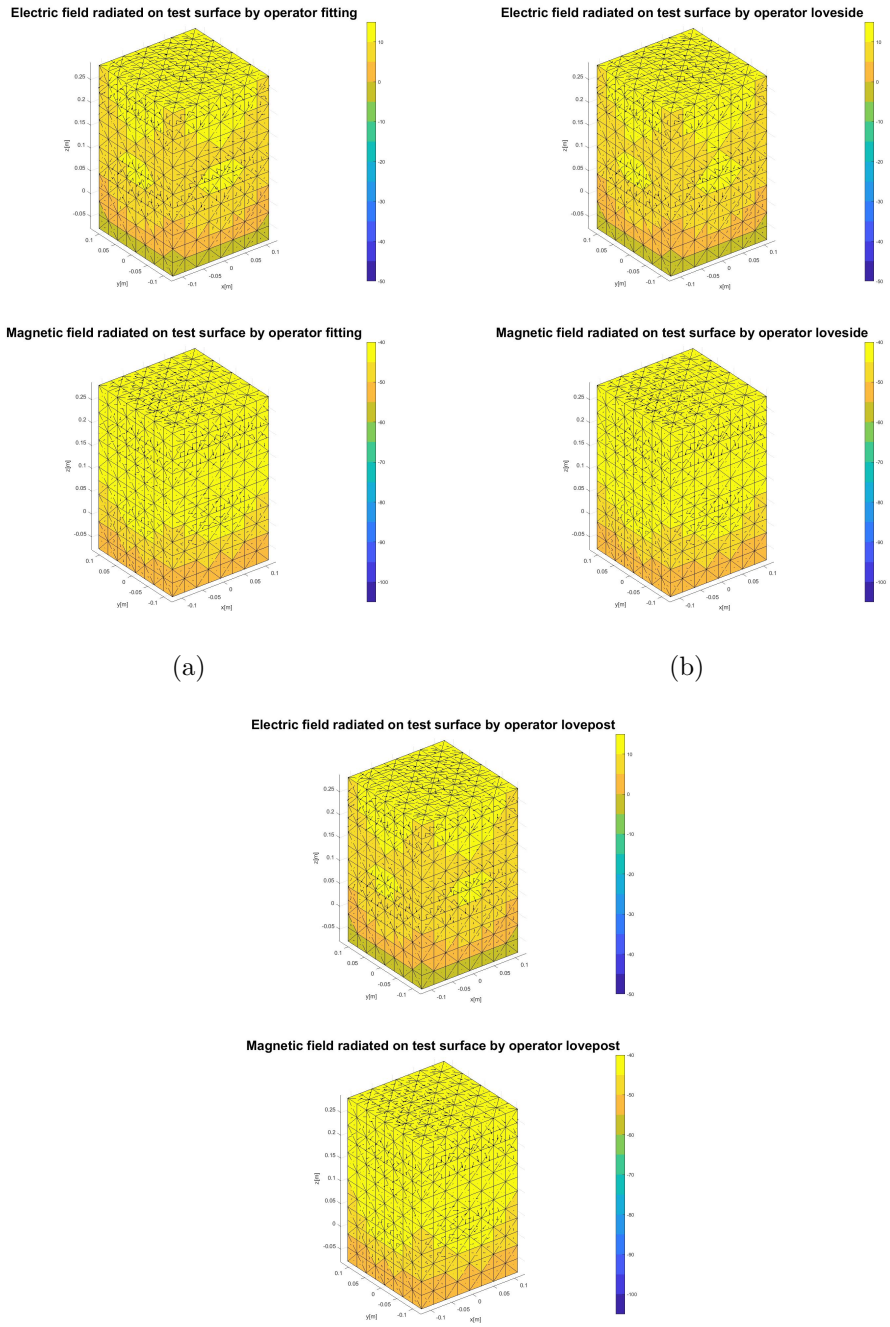

Figure 4.5: Field radiated on test surface when SNR set to 45. *Fitting* refers to the J_{eq}^{F} in Eq(2.8),*Loveside* refers to the J_{eq}^{S} in Eq(2.9),*Lovepost* refers to the J_{eq}^{P} in Eq(2.10). (a)Fitting(b)Loveside(c)Lovepost.

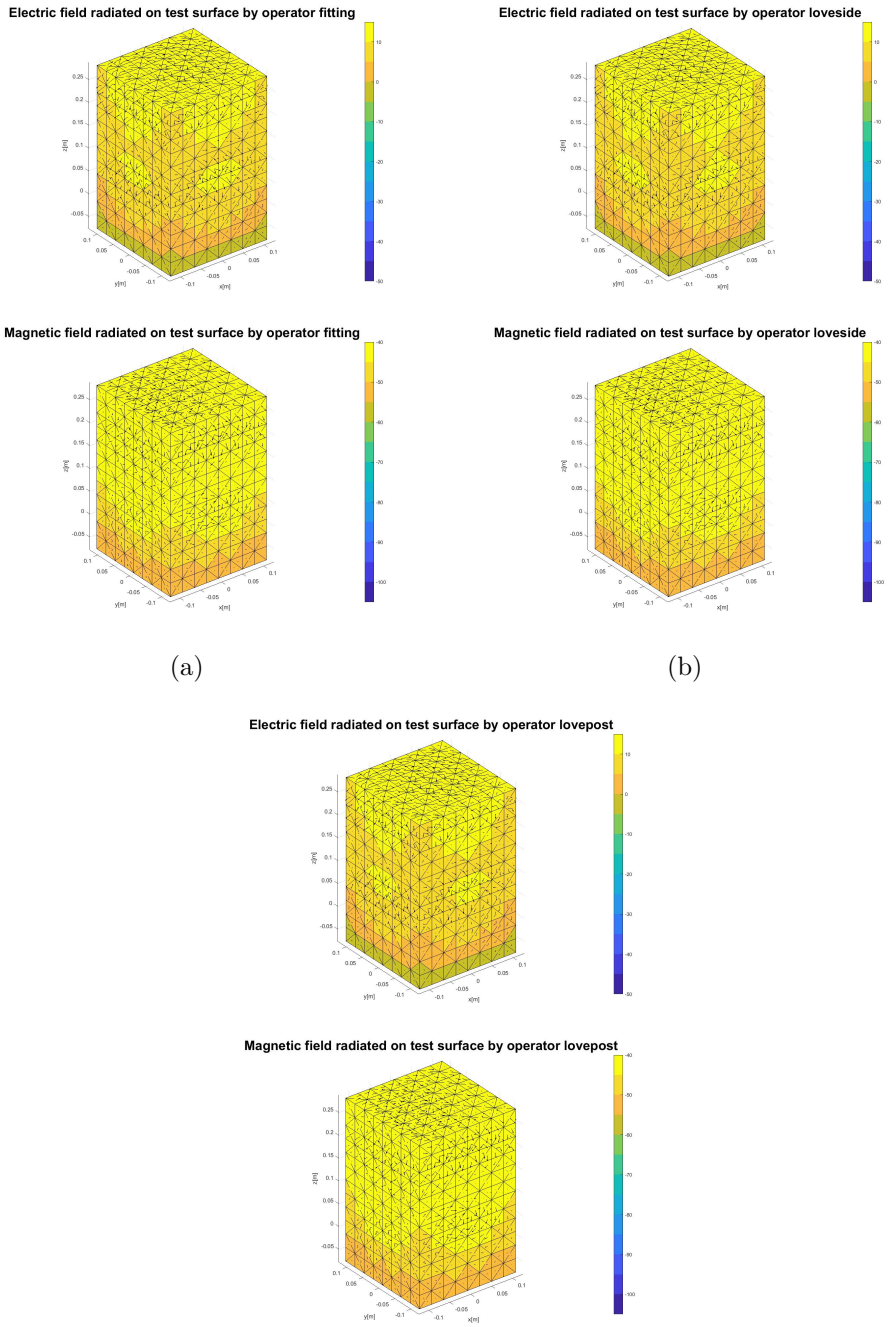

Figure 4.6: Field radiated on test surface when SNR set to 60.*Fitting* refers to the J_{eq}^{F} in Eq(2.8),*Loveside* refers to the J_{eq}^{S} in Eq(2.9),*Lovepost* refers to the J_{eq}^{P} in Eq(2.10). (a)Fitting(b)Loveside(c)Lovepost.

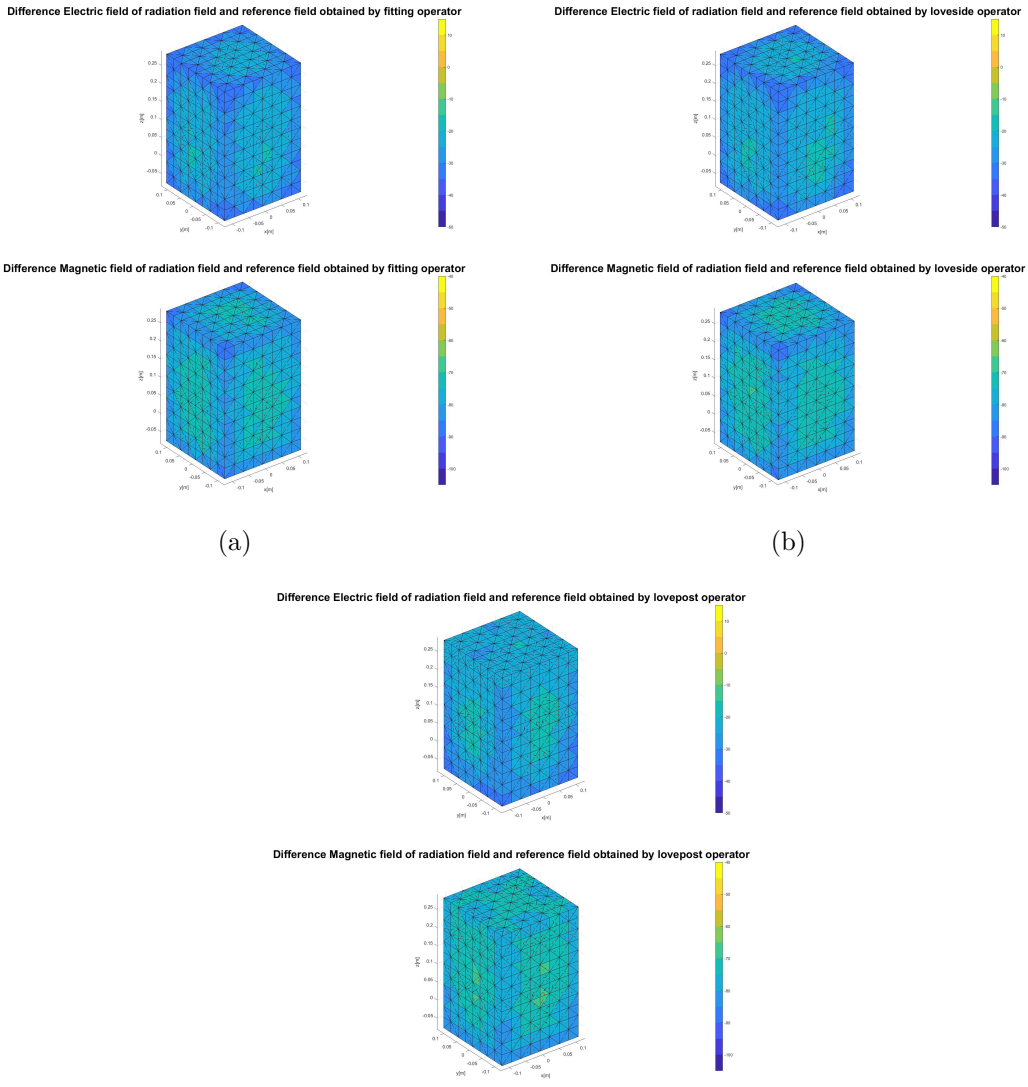

Figure 4.7: Error of the field radiated on test surface when SNR set to 30.*Fitting* refers to the J_{eq}^{F} in Eq(2.8),*Loveside* refers to the J_{eq}^{S} in Eq(2.9),*Lovepost* refers to the J_{eq}^{P} in Eq(2.10). (a)Fitting(b)Loveside(c)Lovepost.

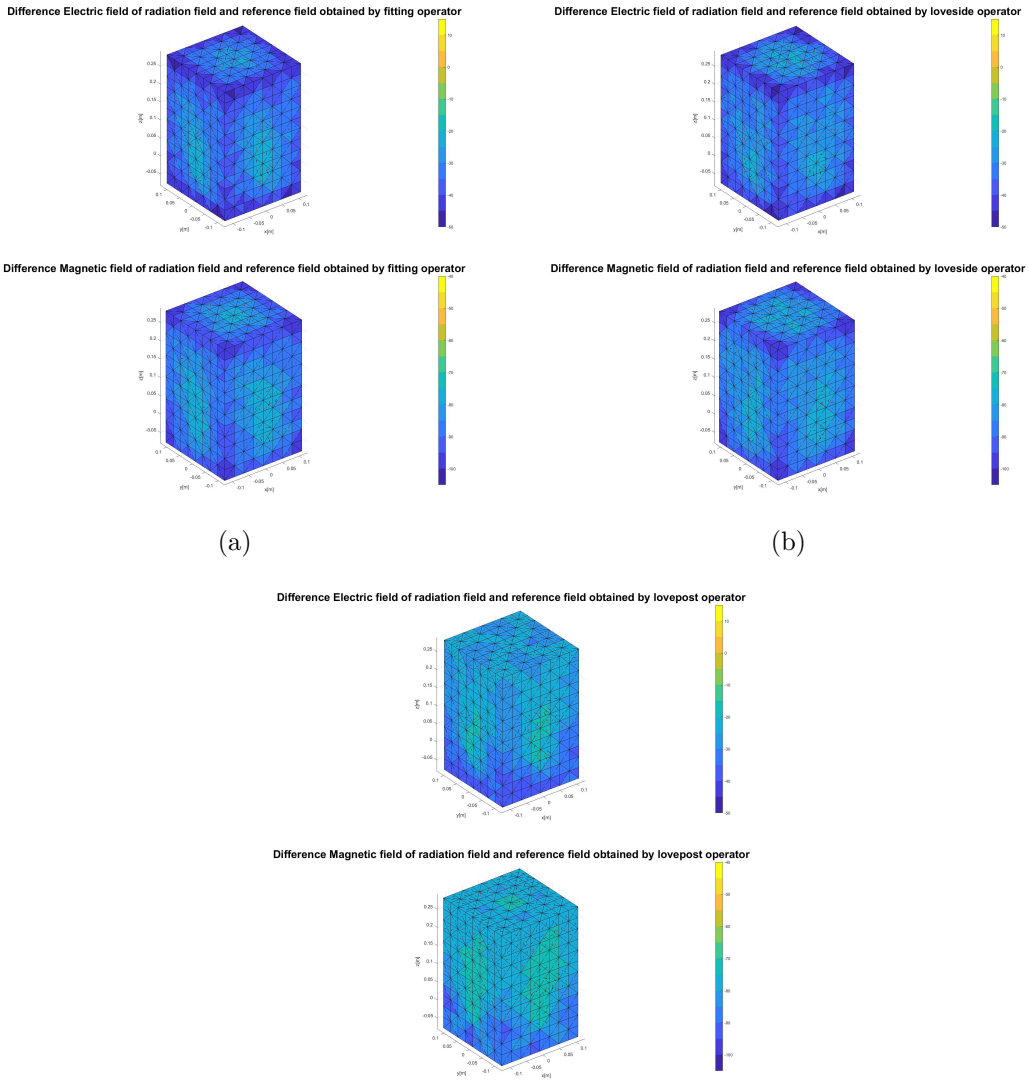

Figure 4.8: Error of the field radiated on test surface when SNR set to 45. *Fitting* refers to the J_{eq}^{F} in Eq(2.8),*Loveside* refers to the J_{eq}^{S} in Eq(2.9),*Lovepost* refers to the J_{eq}^{P} in Eq(2.10). (a)Fitting(b)Loveside(c)Lovepost.

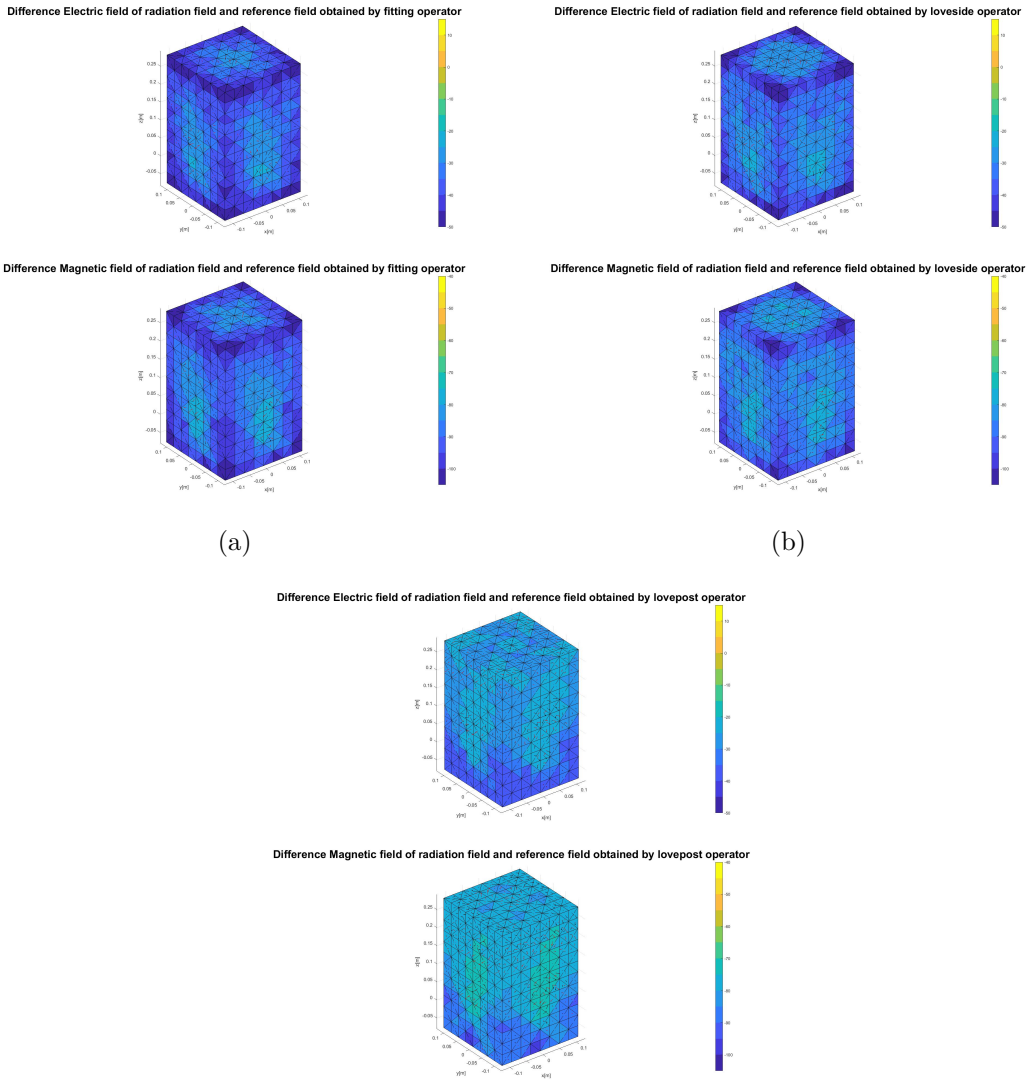

Figure 4.9: Error of the field radiated on test surface when SNR set to 60. *Fitting* refers to the J_{eq}^{F} in Eq(2.8),*Loveside* refers to the J_{eq}^{S} in Eq(2.9),*Lovepost* refers to the J_{eq}^{P} in Eq(2.10). (a)Fitting(b)Loveside(c)Lovepost.

Chapter 5

RUNNING TIME

The time to solve the system and the time to fill the matrices shows in table 5.1.

METHOD	MATRICES								TOTAL
	EJ+EM	EFIE	nxEFIE	HFIE	nxHFIE	G G_{nx}	lsqr	CALDERON	
FITTING	3505.16						5.25		3510.41
LOVEPOST	3505.16		360.68	4149.06		1.61	5.25	0.24	8022
LOVESIDE	3505.16	89.41			3716.24	1,61	14.97		7327.39

Table 5.1: The time for different methods fill the matrix they need and their running time for computing lsqr. Unit[s].

Where EJ and EM are the electric fields on the measurement surface obtained from electric current samples and magnetic current samples which considering quadrature weight, they are used to obtain radiation matrices, see Eq. 2.8. EFIE (Electric Field Integral Equation) and HFIE (Magnetic Field Integral Equation) are the matrices for computing the electric field and magnetic field on reconstruction surface, see Eq. 2.10 and 2.9. $\hat{n}$ is the unit normal vector on surface Σ_R. G and G_{nx} represents Gram matrix. lsqr is an iterative solver inversion to compute the coefficient for three kinds of operators which use different equations. CALDERON is the matrix to invert G to get love current from re-irradiated field for *Lovepost*.

Three sets of equivalent electric and magnetic currents, each one obtained solving an inverse problem satisfying different equations. For *Fitting* it only takes time to build radiation matrices and lsqr, but for *Lovepost* it takes time not only to build radiation matrices and lsqr, but also to get nxEFIE and HFIE and CALDERON. For *Loveside* it is necessary to get nxHFIE and EFIE while obtaining build radiation matrices and lsqr.

As shown in table 5.1, the shortest running time is 3510.14 s for *Fitting*, followed by 7327.39 s for *Loveside*, with a running time of The longest is *Lovepost* with a running duration of 8022 s.

Chapter 6

CONCLUSION

This manuscript introduces and discusses the performance of three different algorithms of the operator for the equivalent inverse current problem with noise in the environment as a parameter. The operator using the *Fitting* logic and algorithm performs better for the accuracy of the field of the reconstructed field (high accuracy on the re-irradiated field); the operator using the *Lovepost* logic and algorithm performs better for the information about the currents on the reconstructed field and the power flux (high adherence to the equivalent currents fulfilling Love's condition). The operator labelled as *Loveside* gives trade-off between accuracy of the re-irradiated field and the adherence with the true equivalent currents fulfilling Love's condition. In the future, depending on the requirements and environmental conditions, a more suitable operator can be used to do the job better. Most of the practical systems are associated with SNR values of 30 dB to 60 dB and interestingly our operators *Fitting*, *Loveside* and *Lovepost* perform very well in this SNR range. In the work that follows, there are a number of questions that are worth discussing: for example, does the performance of the three operators change for different antenna models? And the question of the hardware cost of the three different operators in practical applications.

Bibliography

[1] F. Las-Heras, M.R. Pino, S. Loredo, Y. Alvarez, and T.K. Sarkar. «Evaluating near-field radiation patterns of commercial antennas». In: *IEEE Transactions on Antennas and Propagation* 54.8 (2006), pp. 2198–2207. DOI: 10.1109/TAP.2006.879190 (cit. on p. 1).

[2] Yuri Alvarez, Fernando Las-Heras, and Marcos RodrÍguez Pino. «Reconstruction of Equivalent Currents Distribution Over Arbitrary Three-Dimensional Surfaces Based on Integral Equation Algorithms». In: *IEEE Transactions on Antennas and Propagation* 55.12 (2007), pp. 3460–3468. DOI: 10.1109/TAP.2007.910316 (cit. on p. 1).

[3] MM Leibfritz, FM Landstorfer, and TF Eibert. «An equivalent source method to determine complex excitation levels of antenna arrays from near-field measurements». In: (2007) (cit. on p. 1).

[4] Yuri Alvarez, Tapan K Sarkar, and Fernando Las-Heras. «Improvement of the sources reconstruction techniques: Analysis of the svd algorithm and the rwg basis functions». In: *2007 IEEE Antennas and Propagation Society International Symposium*. IEEE. 2007, pp. 5644–5647 (cit. on p. 1).

[5] Javier Leonardo, Araque Quijano, and Giuseppe Vecchi. «Removal of unwanted structural interactions from antenna measurements». In: *2009 IEEE Antennas and Propagation Society International Symposium*. 2009, pp. 1–4. DOI: 10.1109/APS.2009.5172309 (cit. on p. 1).

[6] Javier Leonardo Araque Quijano and Giuseppe Vecchi. «Improved-Accuracy Source Reconstruction on Arbitrary 3-D Surfaces». In: *IEEE Antennas and Wireless Propagation Letters* 8 (2009), pp. 1046–1049. DOI: 10.1109/LAWP.2009.2031988 (cit. on p. 1).

[7] Javier Leonardo Araque Quijano and Giuseppe Vecchi. «Field and source equivalence in source reconstruction on 3D surfaces». In: *Progress In Electromagnetics Research* 103 (2010), pp. 67–100 (cit. on pp. 1, 4).

[8] Jonas Kornprobst, Raimund AM Mauermayer, Ole Neitz, Josef Knapp, and Thomas F Eibert. «On the solution of inverse equivalent surface-source problems». In: *Progress In Electromagnetics Research* 165 (2019), pp. 47–65 (cit. on p. 1).